ELECTRON-HOLE EXCHANGE INTERACTION IN THE NON-CONCENTRIC SPHERICAL CORE-SHELL QUANTUM DOT

R. Ya. Leshko[1] , O. V. Leshko[1] , I. V. Bilynskyi[1,2] , R. I. Pazyuk[1]

[1] *Department of Physics and Information Systems,*
Drohobych Ivan Franko State Pedagogical University,
3, Stryiska St., Drohobych, UA–82100, Ukraine,
[2] *Department of Physics, Kryvyi Rih State Pedagogical University,*
54, University Ave., Kryvyi Rih, UA–50086, Ukraine
e-mail: leshkoroman@gmail.com

In this work we investigated the effect of the non-concentricity parameter on the magnitude of the exciton dark-light splitting in spherical non-concentric CdSe/CdS core-shell quantum dots. Quantum dots with both narrow and wide shells have been investigated. It has been shown that as the shell radius increases, the exchange interaction energy decreases and the exciton dark-light splitting decreases too. However, with fixed core and shell sizes, the core displacement from the common center leads to a monotonic increase in the exchange interaction for small shell radii and to a non-monotonic increase for larger shell radii. The obtained results are consistent with experimental data.

Key words: core-shell quantum dot, non-concentricity parameter, exciton dark-light splitting.

I. INTRODUCTION

Modern demands for high energy efficiency and low energy consumption drive researchers to develop new devices based on novel organic and inorganic materials. These include solar panels, detectors, sources of electromagnetic radiation, and solar concentrators. Solar luminescent concentrators based on quantum dots (QDs), which have high efficiency in collecting solar energy, deserve special attention [1]. As shown in work [2], core-shell quantum dots (CSQDs) are particularly effective for solar concentrators. The application of CdSe/CdS quantum dots as luminescent centers has made it possible to achieve the luminescence quantum efficiency (LQE) 86% [2]. These CSQDs exhibit substantial absorption cross-sections and adjustable emission properties determined by the size of CSQDs. Additionally, colloidal CSQDs offer improved photostability compared to organic chromophores and can be integrated into organic or inorganic matrices through solution-based methods. Also PbS/CdS CSQDs have large LQE of 50% [3] and 70% [4]. This efficiency is achieved because CdSe/CdS and PbS/CdS CSQDs have a significant difference between the absorption and luminescence bands. Simple CdSe QDs do not have a large value of the Stokes shift [5–7]. The Stokes shift can be increased in the CSQD by separating electrons and holes in different regions of the QD. It can be achieved in the CSQD of the II type or in the CSQD of the I type with an especially thick shell, like CdSe/CdS CSQD, (types of the QD are presented in [8]]). In summary, the QDs with a large Stokes shift are a promising candidate for use in solar concentrators.

Given the aforementioned, the Stokes shift in QDs is an important physical effect that underlies the construction of solar luminescent concentrators. There are various reasons for the Stokes shift in quantum dots. One of the reasons is the electron–hole exchange interaction, which causes exciton dark-light splitting [5]. The mechanism of the Stokes shift in semiconductor QDs has been analyzed and discussed in [9]. The influence of polarization and deformation on the electron–hole exchange interaction has been analyzed in [10]. There, in [10], it shown that these two opposite effects (polarization and deformation) in the InAs/GaAs QD partially offset each other. In other heterostructures with QDs (where the dielectric permittivities and lattice constants of the media are close to each other), the effects of strain and polarization practically do not influence the exciton dark-light splitting.

No matter what QD growth technologies are used (for example, [11–13]), there is always a chance that the core will be off-center, especially in the case of a thick shell. The use of colloidal technologies allows for the production of approximately spherical QDs. Therefore, in most cases, spherical non-concentric CSQDs are obtained. Since the core size and shell thickness affect the energy spectra of electrons and holes, these dimensions will consequently influence the magnitude of the Stokes shift. As shown in [14, 15], the energy spectra also depend on the non-concentricity parameter. Also it was defined that the non-concentricity parameter has an effect on the interband absorption [16]. Given this, it is logical to assume that the non-concentricity parameter will also affect the exciton dark-light splitting in spherical non-concentric CSQDs. This very issue is the focus of the proposed work.

II. THEORY OF ELECTRON (HOLE) STATES

A non-concentric CSQD is considered. The radius of the core is r_0, and the radius of the shell is r_1. We assume that the core is displaced from the common center by a distance D along the z-axis (see Fig. 1). Also we consider condition $D \leq r_1 - r_0$.
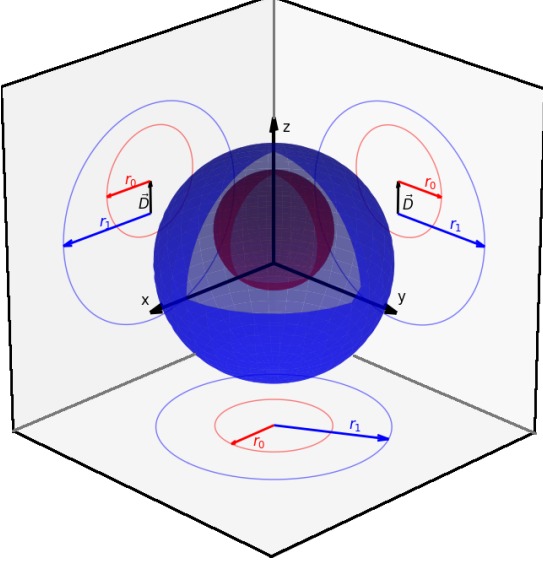
Fig. 1. The geometric model of the spherical non-concentric CSQD

The Hamiltonian of the electron (hole) within the framework of the effective mass method has the form:

$$\widehat{H} = -\boldsymbol{\nabla} \cdot \left(\frac{m_0}{m(\mathbf{r})} \boldsymbol{\nabla} \right) + U(\mathbf{r}). \tag{1}$$

In this work, the position-dependent effective mass

Hamiltonian is reduced to the most common BenDaniel–Duke form [17]. More complex models of the effective Hamiltonian with a position-dependent mass with ordering problem, like in [18–20] are not consided. Also the proposed Hamiltonian (1) is written in units of effective Rydberg energy $\mathrm{Ry}^* = \hbar^2 / \left(2m_0 a_b^{*2} \right)$ and effective Bohr radius $a_b^* = \left(\hbar^2 \varepsilon \right) / \left(m_0 e^2 \right)$, m_0 is an electron effective mass in core, $\varepsilon = (\varepsilon_0 + \varepsilon_1)/2$ is the average dielectric permittivity, $\hbar$ is the Planck constant, e is the elementary charge,

$$m(\mathbf{r}) = \begin{cases} m_0, & \mathbf{r} \in \text{core}, \\ m_1, & \mathbf{r} \in \text{shell}, \\ m_2, & \mathbf{r} \in \text{matrix} \end{cases} \tag{2}$$

is the effective electron (hole) mass,

$$U(\mathbf{r}) = \begin{cases} 0, & \mathbf{r} \in \text{core}, \\ U_1, & \mathbf{r} \in \text{shell}, \\ U_2, & \mathbf{r} \in \text{matrix} \end{cases} \tag{3}$$

is the confinement potential for electron (hole), $U_2 > U_1$. If we consider electron states, the masses are as follows: $m_0 = m_0^{\mathrm{e}}$, $m_1 = m_1^{\mathrm{e}}$, $m_2 = m_2^{\mathrm{e}}$, $U_1 = U_1^{\mathrm{e}}$, $U_2 = U_2^{\mathrm{e}}$. For hole states, we use $m_0 = m_0^{\mathrm{h}}$, $m_1 = m_1^{\mathrm{h}}$, $m_2 = m_2^{\mathrm{h}}$, $U_1 = U_1^{\mathrm{h}}$, $U_2 = U_2^{\mathrm{h}}$.

To determine the energy spectrum and wave functions of an electron (hole) in the spherical non-concentric CSQD, it is necessary to solve the Schrödinger equation using Hamiltonian (1). However, finding exact analytical solutions for the Schrödinger equation in this case, where $D \neq 0$, is not feasible. That's why we use the plane wave approach [14, 21, 22]. According to this method, the wave function can be represented as follows

$$\psi(\mathbf{r}) = \sum_{n_x, n_y, n_z} C_{n_x, n_y, n_z} \psi_{n_x, n_y, n_z}^{(0)}(x, y, z), \tag{4}$$

where

$$\psi_{n_x, n_y, n_z}^{(0)}(x, y, z) = \frac{1}{\sqrt{L^3}} \exp \left\{ i \left[(k_x + n_x K_x) x + (k_y + n_y K_y) y + (k_z + n_z K_z) z \right] \right\}, \tag{5}$$

L represents the length of the unit cell's edge in the x, y, and z directions within the coordinate system,

$$K_x = K_y = K_z \equiv 2\pi/L, \tag{6}$$

$$n_x \in [-n_{\max}, \ldots, n_{\max}], \qquad n_y \in [-n_{\max}, \ldots, n_{\max}], \qquad n_z \in [-n_{\max}, \ldots, n_{\max}]. \tag{7}$$

Studies [14, 21, 22] showed that convergence was achieved with parameters $n_{\max} = 7$ and $L = 2.5 + 2r_1$. Additionally, it was verified that the results are not influenced by the wave vector components (k_x, k_y, k_z) under

these conditions. Therefore, for the following computations, we set $k_x = k_y = k_z = 0$.

By substituting wave function (4) into the Schrödinger equation with Hamiltonian (1), we obtain the following

system of linear homogeneous equations:

$$\sum_{n_x, n_y, n_z} \left(T_{\substack{n'_x, n'_y, n'_z \\ n_x, n_y, n_z}} + U_{\substack{n'_x, n'_y, n'_z \\ n_x, n_y, n_z}} - E\delta_{\substack{n'_x, n'_y, n'_z \\ n_x, n_y, n_z}} \right)$$

$$\times C_{n_x, n_y, n_z} = 0. \tag{8}$$

Matrix element $T_{\substack{n'_x, n'_y, n'_z \\ n_x, n_y, n_z}}$ is presented in the appendix and $U_{\substack{n'_x, n'_y, n'_z \\ n_x, n_y, n_z}}$ was presented and derived in the work [14] for the spherical non-concentric CSQD.

The electron (hole) energy E and all coefficients C_{n_x, n_y, n_z} can be calculated using the system of linear homogeneous equations (8) and with the normalization condition $\sum_{n_x, n_y, n_z} |C_{n_x, n_y, n_z}|^2 = 1$. As a result, the wave function (4) can be determined.

III. THE EXCITON DARK-LIGHT SPLITTING

The electron–hole exchange interaction is given in [5, 10]:

$$\hat{H}_{\text{ex}} = -(2/3)\varepsilon_{\text{exch}}(a_0)^3 \delta(\mathbf{r}_e - \mathbf{r}_h)(\boldsymbol{\sigma}_e \cdot \mathbf{J}_h)$$

$$= -\alpha\delta(\mathbf{r}_e - \mathbf{r}_h)(\boldsymbol{\sigma}_e \cdot \mathbf{J}_h), \tag{9}$$

where a_0 is the QD lattice parameter, $\varepsilon_{\text{exch}}$ is the exchange strength constant, which can be defined from equation [5]:

$$\hbar\omega_{\text{st}} = (8/3\pi)(a_0/a_{\text{ex}})^3 \varepsilon_{\text{exch}}, \tag{10}$$

a_{ex} is the exciton radius, $\hbar\omega_{\text{st}} = 0.13$ meV [5]. $\boldsymbol{\sigma}_e$ is the electron Pauli spin-1/2 matrix, $\mathbf{J}_h$ is the hole spin matrix. In the case of the singleband hole model, the hole spin equals to 1/2.

To define the exchange interaction, we use the electron–hole wave function in the form:

$$\psi_{\text{ex}}(\mathbf{r}_{\text{el}}, \mathbf{r}_h) = \sum_{s_z=-1/2}^{1/2} \sum_{j_z=-1/2}^{1/2} c_{s_z, j_z} \psi_{\text{el}}(\mathbf{r}_{\text{el}}) \chi_{\text{el}; s_z}$$

$$\times \psi_h(\mathbf{r}_h) \chi_{h; j_z}. \tag{11}$$

where χ is the spin function. Using function (11), the matrix of the electron–hole exchange interaction will take the form [10]:

$$\begin{pmatrix} Z & 0 & 0 & 0 \\ 0 & -Z & 2Z & 0 \\ 0 & 2Z & -Z & 0 \\ 0 & 0 & 0 & Z \end{pmatrix}, \tag{12}$$

where

$$Z = \alpha \int |\psi_{\text{el}}(\mathbf{r})|^2 |\psi_h(\mathbf{r})|^2 \, d\mathbf{r}. \tag{13}$$

The eigenvalues of (12) define the electron–hole exchange interaction. Therefore we get four eigenvalues. Three of them are equal to Z. This corresponds to an optically active state (light states) with the total electron–hole spin momentum equal to 1. One eigenvalue is equal to $-3Z$ (total electron–hole spin momentum is equal to 0). This is a dark state. Therefore, the splitting energy is $E_s = 4Z$.

IV. RESULTS DISCUSSION

The calculations were carried out for the spherical core-shell quantum dot CdSe/CdS, using the parameters specified in [6, 7]. Effective masses $m_0^e = 0.13m_e$, $m_1^e = 0.21m_e$, $m_2^e = m_e$ [6]; $m_0^h = 0.45m_e$, $m_1^h = 0.68m_e$, $m_2^h = m_e$ [6]. Here, m_e is a free electron mass. The conduction-band and valency-band energy offset $U_1^e = 320$ meV and $U_1^h = 430$ meV [6]. We chose the confinement potential on the boundary shell-matrix to be very large $U_1^e = U_2^h = 2000$ meV. First of all, we calculated the dependence of the electron and hole energy on the core displacement parameter D for different values of the shell radius while keeping the core size fixed $r_0 = 15$ Å. This particular size has been considered in the works [6, 7]. Also in these works, the shell thickness has been obtained:

A) $h = 8$ Å ($r_1 = 23$ Å);

B) $h = 16$ Å ($r_1 = 31$ Å);

C) $h = 28$ Å ($r_1 = 43$ Å);

D) $h = 56$ Å ($r_1 = 71$ Å).

We assume that in these and other samples, concentricity may be disrupted. That is why the electron and hole energies are functions of D. The dependence of both electron and hole ground state energies on D is presented in Fig. 2.

From Fig. 2, it can be seen that the energy of the electron and hole increases as the QD core shifts away from the common center. However, as the shell radius increases, this dependence becomes less pronounced. This dependence is due to the fact that the electron and hole are less influenced by the second heterointerface (shell-matrix). This results are in good agreement with the ones in [14, 16].

The relative shift in the positions of the electron and hole wave functions will cause a change in the electron–hole exchange interaction. The results of the calculated dependence of the electron–hole interaction on the parameter D are presented in Fig. 3.

From Fig. 3, it can be seen that the electron–hole exchange interaction in concentric core-shell QD ($D = 0$) decreases if the shell thickness increases from 23 to 71 Å. These results are in good qualitative agreement with the experimental results published in [6]. Also one can see the monotonous growth in the exchange energy with increasing D for core-shell QD with small and medium shell radius ($r_1 = 23$ Å and $r_1 = 31$ Å). If the shell radius is large

(for example, $r_1 = 43$ Å or $r_1 = 71$ Å), non-monotonous dependence is observed. This dependence can be explai-

ned based on the probability density distribution of the electron and hole in the core-shell QD (Figs. 4 and 5).
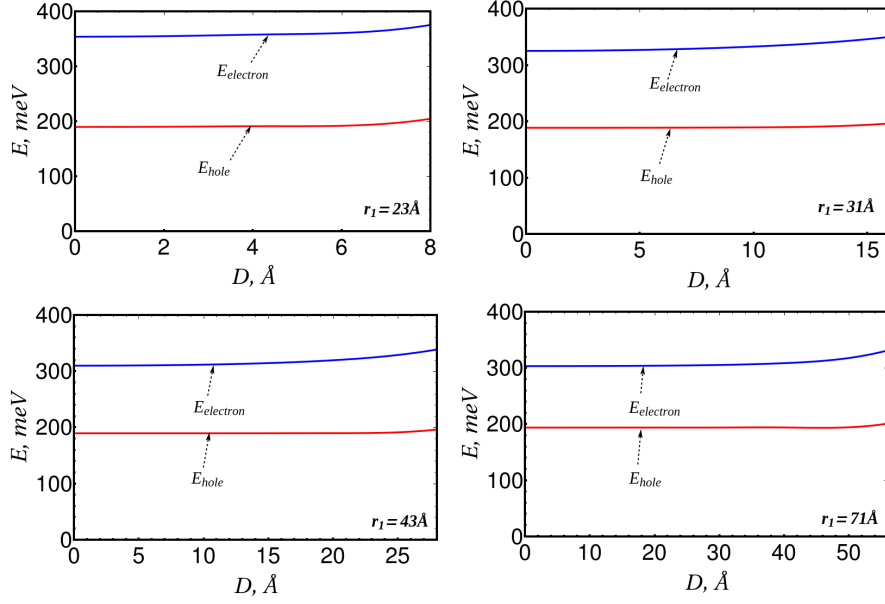
Рис. 2. Electron and hole ground state energy as a functions of the core displacement D for different shell radii
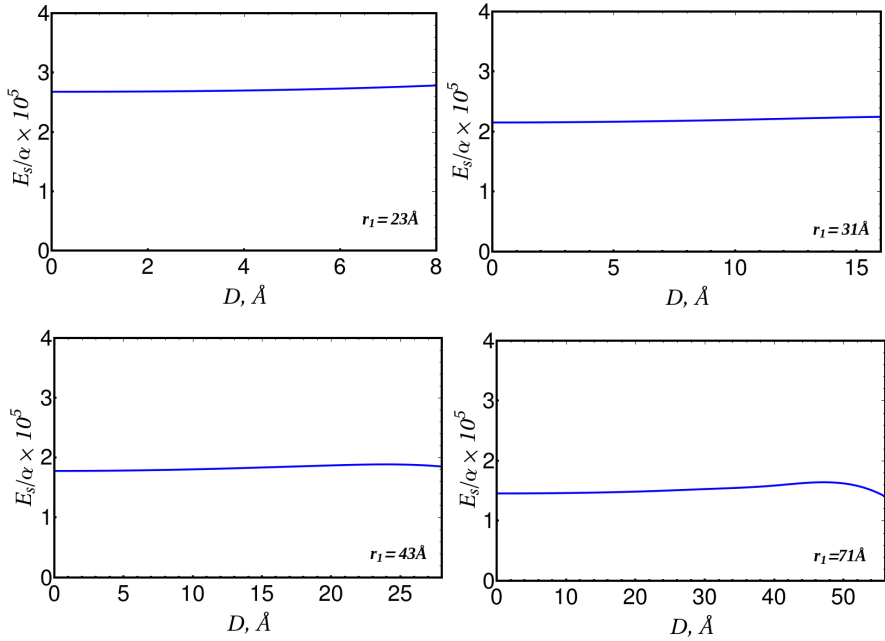
Рис. 3. The energy of exciton dark-light splitting as a function of the core displacement D for different shell radii

As the shell thickness increases (for a concentric CSQD), the electron wave function penetrates from the core into the shell due to the shallow potential well in the QD core. For the hole, the corresponding potential well is deeper, and the effective mass of the hole is larger, resulting in a more localized wave function within the core. Consequently, the overlap of the wave functions decreases, leading to a reduction in integral (13). Therefore, the exchange interaction in concentric spherical core-shell quantum dots decreases with the increase in shell thickness. However, with fixed core and

shell sizes, the displacement of the core is accompanied by an increase in exchange energy. For example, in the case of $r_1 = 23$ Å, the overlap of the electron and hole wave functions increases monotonically with core displacement. This is due to the fact that the electron also experiences the influence of the shell-matrix boundary with any core displacement. In the case of $r_1 = 43$ Å, the electron does not immediately experience the influence of the shell-matrix boundary, so the increase is slow and almost unnoticeable with core displacement. However, when the displacement becomes significant (see Fig. 5.3e)

and the core approaches the shell-matrix boundary, this influence becomes noticeable, and the electron's wave function is pushed out of the core to the opposite side of the displacement. For the hole, a similar situation is not observed because the hole is much more strongly confined by the potential well. As a result, the overlap of the wave functions decreases, leading to a reduction in the exchange interaction (Fig. 3, $r_1 = 43$ Å and $r_1 = 71$ Å).
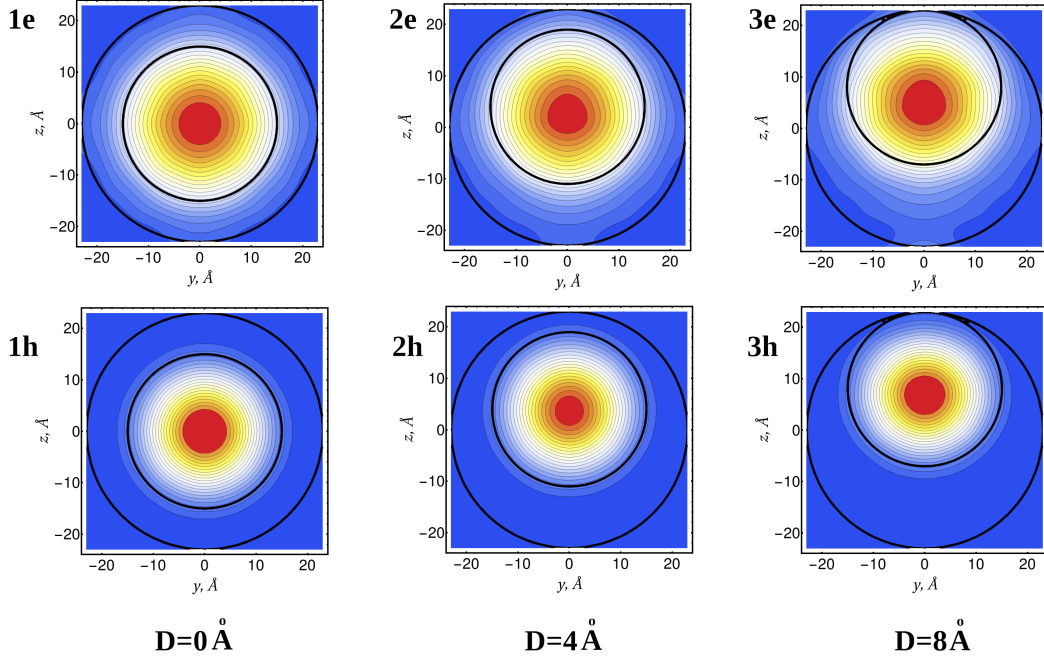
Рис. 4. The probability density distribution of the electron (1e, 2e, 3,e) and hole (1h, 2h, 3h) in the core-shell QD. Shell radius is $r1 = 23$ Å
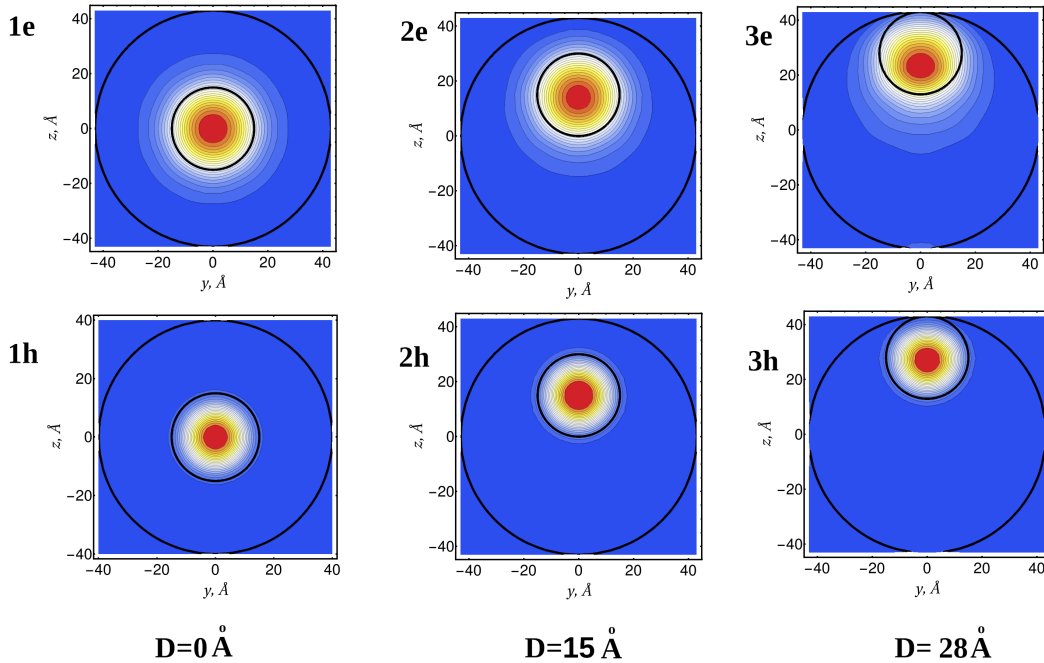
Рис. 5. The probability density distribution of the electron (1e, 2e, 3,e) and hole (1h, 2h, 3h) in the core-shell QD. Shell radius is $r_1 = 43$ Å

V. CONCLUSION

Thus, in this work, a spherical non-concentric CSQD has been studied using the plane-wave method. The ground-state energies of the electron and hole are determined. The dependence of these energies on the shell thickness and the position of the core in the quantum dot is analyzed. It is shown that the displacement of the core from the common center causes an increase in the energy of both the electron and the hole. For QDs with a larger shell radius, this increase occurs more slowly than for QDs with a smaller shell radius. Based on the obtained wave functions of the electron and hole, the exchange interaction energy, which defines the splitting of dark and bright states, is calculated. It is shown that the exchange interaction energy decreases with increasing shell radius, while the core displacement from the quantum dot center causes an increase in the exchange interaction energy. Moreover, for small shell radii, the exchange interaction energy increases monotonically, while for larger radii, it increases non-monotonically. The reason for this dependence lies in the mutual spatial arrangement of the electron and hole wave functions in the QD. The obtained results qualitatively agree with experimental studies. To improve the convergence of the results, the model can be extended to account for the complex structure of the valence band, which will be implemented in our subsequent work.

APPENDIX

$$T_{\substack{n_x', n_y', n_z' \\ n_x, n_y, n_z}} = -\int_{-L/2}^{L/2} \int_{-L/2}^{L/2} \int_{-L/2}^{L/2} \psi_{n_x', n_y', n_z'}^{(0)*}(x, y, z) \boldsymbol{\nabla} \frac{m_0}{m(\mathbf{r})} \boldsymbol{\nabla} \psi_{n_x, n_y, n_z}^{(0)}(x, y, z)\, dV.$$

We take into account the Hermiticity of the momentum operator (in the chosen coordinate system it has the form $-i\boldsymbol{\nabla}$). After transformations and using (5), we get

$$T_{\substack{n_x', n_y', n_z' \\ n_x, n_y, n_z}} = \frac{1}{L^3}\big[(k_x + n_x' K_x)(k_x + n_x K_x) + (k_y + n_y' K_y)(k_y + n_y K_y) + (k_z + n_z' K_z)(k_z + n_z K_z)\big]$$

$$\times \int_{-L/2}^{L/2} \int_{-L/2}^{L/2} \int_{-L/2}^{L/2} \frac{m_0}{m(\mathbf{r})} \exp\left\{i\boldsymbol{\lambda}\cdot\mathbf{r}\right\} dV,$$

where $\boldsymbol{\lambda} = \frac{2\pi}{L}(\mathbf{i}(n_x - n_x') + \mathbf{j}(n_y - n_y') + \mathbf{k}(n_z - n_z'))$. According to (6) and $k_x = k_y = k_z = 0$, we get

$$T_{\substack{n_x', n_y', n_z' \\ n_x, n_y, n_z}} = \frac{1}{L^3}\left(\frac{2\pi}{L}\right)^2 \big[n_x' n_x + n_y' n_y + n_z' n_z\big] \int_{-L/2}^{L/2} \int_{-L/2}^{L/2} \int_{-L/2}^{L/2} \frac{m_0}{m(\mathbf{r})} \exp\left\{i\boldsymbol{\lambda}\cdot\mathbf{r}\right\} dV.$$

The next step is to calculate the integral.

$$I = \int_{-L/2}^{L/2} \int_{-L/2}^{L/2} \int_{-L/2}^{L/2} \frac{m_0}{m(\mathbf{r})} e^{i\boldsymbol{\lambda}\cdot\mathbf{r}}\, dV = \int_{\text{in matrix}} \frac{m_0}{m_2} e^{i\boldsymbol{\lambda}\cdot\mathbf{r}}\, dV + \int_{\text{in shell}} \frac{m_0}{m_1} e^{i\boldsymbol{\lambda}\cdot\mathbf{r}}\, dV + \int_{\text{in core}} \frac{m_0}{m_0} e^{i\boldsymbol{\lambda}\cdot\mathbf{r}}\, dV.$$

Let us add and subtract the integral over the ball r_1:

$$I = \int_{\text{in matrix}} \frac{m_0}{m_2} e^{i\boldsymbol{\lambda}\cdot\mathbf{r}}\, dV + \int_{\text{in ball } r_1} \frac{m_0}{m_2} e^{i\boldsymbol{\lambda}\cdot\mathbf{r}}\, dV - \int_{\text{in ball } r_1} \frac{m_0}{m_2} e^{i\boldsymbol{\lambda}\cdot\mathbf{r}}\, dV$$

$$+ \int_{\text{in shell}} \frac{m_0}{m_1} e^{i\boldsymbol{\lambda}\cdot\mathbf{r}}\, dV + \int_{\text{in core}} \frac{m_0}{m_0} e^{i\boldsymbol{\lambda}\cdot\mathbf{r}}\, dV.$$

Combine the first and second terms:

$$I = \int_{\text{in box } L} \frac{m_0}{m_2} e^{i\boldsymbol{\lambda}\cdot\mathbf{r}}\, dV - \int_{\text{in ball } r_1} \frac{m_0}{m_2} e^{i\boldsymbol{\lambda}\cdot\mathbf{r}}\, dV + \int_{\text{in shell}} \frac{m_0}{m_1} e^{i\boldsymbol{\lambda}\cdot\mathbf{r}}\, dV + \int_{\text{in core}} \frac{m_0}{m_0} e^{i\boldsymbol{\lambda}\cdot\mathbf{r}}\, dV.$$

Due to the fact that the system of plane waves in a cube of length L is orthonormal, we have:

$$I = L^3 \delta_{n_x', n_x} \delta_{n_y', n_y} \delta_{n_z', n_z} - \int_{\text{in ball } r_1} \frac{m_0}{m_2} e^{i\boldsymbol{\lambda}\cdot\mathbf{r}}\, dV + \int_{\text{in shell}} \frac{m_0}{m_1} e^{i\boldsymbol{\lambda}\cdot\mathbf{r}}\, dV + \int_{\text{in core}} \frac{m_0}{m_0} e^{i\boldsymbol{\lambda}\cdot\mathbf{r}}\, dV.$$

Let us add and subtract the other integral:

$$I = L^3 \delta_{n'_x,n_x} \delta_{n'_y,n_y} \delta_{n'_z,n_z} \ - \int_{\text{in ball } r_1} \frac{m_0}{m_2} e^{i\boldsymbol{\lambda}\cdot\mathbf{r}} \, dV + \int_{\text{in shell}} \frac{m_0}{m_1} e^{i\boldsymbol{\lambda}\cdot\mathbf{r}} \, dV + \int_{\text{in core}} \frac{m_0}{m_0} e^{i\boldsymbol{\lambda}\cdot\mathbf{r}} \, dV$$

$$+ \int_{\text{in core}} \frac{m_0}{m_1} e^{i\boldsymbol{\lambda}\cdot\mathbf{r}} \, dV - \int_{\text{in core}} \frac{m_0}{m_1} e^{i\boldsymbol{\lambda}\cdot\mathbf{r}} \, dV.$$

The third and fifth terms can be joined:

$$I = L^3 \delta_{n'_x,n_x} \delta_{n'_y,n_y} \delta_{n'_z,n_z} \ - \int_{\text{in ball } r_1} \frac{m_0}{m_2} e^{i\boldsymbol{\lambda}\cdot\mathbf{r}} \, dV + \int_{\text{in ball } r_1} \frac{m_0}{m_1} e^{i\boldsymbol{\lambda}\cdot\mathbf{r}} \, dV + \int_{\text{in core}} \frac{m_0}{m_0} e^{i\boldsymbol{\lambda}\cdot\mathbf{r}} \, dV$$

$$- \int_{\text{in core}} \frac{m_0}{m_1} e^{i\boldsymbol{\lambda}\cdot\mathbf{r}} \, dV.$$

Now the second-third and the fourth-fifth terms can be combined too:

$$I = L^3 \delta_{n'_x,n_x} \delta_{n'_y,n_y} \delta_{n'_z,n_z} + \left(-\frac{m_0}{m_2} + \frac{m_0}{m_1} \right) \int_{\text{in ball } r_1} e^{i\boldsymbol{\lambda}\cdot\mathbf{r}} \, dV + \left(\frac{m_0}{m_0} - \frac{m_0}{m_1} \right) \int_{\text{in core}} e^{i\boldsymbol{\lambda}\cdot\mathbf{r}} \, dV.$$

The calculation of the second integral poses no issues; therefore, we will not provide it. The most interesting part is the last integral, as the core is shifted by the distance D. This integral can be calculated in that way: let $\mathbf{r} = \mathbf{r}' - \mathbf{D}$, and $dx = dx'$, $dy = dy'$, $dz = dz'$, $dV = dV'$. That is why

$$\int_{\text{in core}} e^{i\boldsymbol{\lambda}\cdot\mathbf{r}} \, dV = \int_{\text{in core}} e^{i\boldsymbol{\lambda}\cdot\mathbf{r}' + i\boldsymbol{\lambda}\cdot\mathbf{D}} \, dV' = e^{i\boldsymbol{\lambda}\cdot\mathbf{D}} \int_{\text{in core}} e^{i\boldsymbol{\lambda}\cdot\mathbf{r}'} \, dV'.$$

Such transformations are absolutely valid when $L \to \infty$. For practical use with controlled accuracy, it is necessary to choose a sufficiently large L. Calculations have shown that with the proposed values of L in the main text of the article, the results are convergent.

[1] P. Moraitis, R. E. I. Schropp, W. G. J. H. M. van Sark, Opt. Mater. **84**, 636 (2018); https://doi.org/10.1016/j.optmat.2018.07.034.

[2] F. Meinardi et al., Nat. Photon. **8**, 392 (2014); https://doi.org/10.1038/nphoton.2014.54.

[3] G. V. Shcherbatyuk, R. H. Inman, C. Wang, R. Winston, S. Ghosh, Appl. Phys. Lett. **96**, 191901 (2010); https://doi.org/10.1063/1.3422485.

[4] L. Tan et al., J. Mater. Chem. **5**, 10250 (2017); https://doi.org/10.1039/c7ta01372h.

[5] Al. L. Efros et al., Phys. Rev. B **54**, 4843 (1996); https://doi.org/10.1103/PhysRevB.54.4843.

[6] S. Brovelli et al., Nat. Commun. **2**, 280 (2011); https://doi.org/10.1038/ncomms1281.

[7] F. García-Santamaría et al., Nano Lett. **11**, 687 (2011); https://doi.org/10.1021/nl103801e.

[8] A. Sahu, D. Kumar, J. Alloys Compd. **924**, 166508 (2022); https://doi.org/10.1016/j.jallcom.2022.166508.

[9] A. Bagga, P. K. Chattopadhyay, S. Ghosh, Phys. Rev. B **74**, 035341 (2006); https://doi.org/10.1103/PhysRevB.74.035341.

[10] R. Ya. Leshko, I. V. Bilynskyi, O. V. Leshko, J. Phys. Stud. **26**, 1702 (2022); https://doi.org/10.30970/jps.26.1702.

[11] M. Cirillo et al., Chem. Mater. **26**, 1154 (2014); https://doi.org/10.1021/cm403518a.

[12] K. Surana, I. T. Salisu, R. M. Mehra, B. Bhattacharya, Opt. Mater. **82**, 135 (2018); https://doi.org/10.1016/j.optmat.2018.05.060.

[13] C. Zhou et al., J. Photochem. Photobiol. A Chem. **332**, 251 (2017); https://doi.org/10.1016/j.jphotochem.2016.08.035.

[14] R. Ya. Leshko, I. V. Bilynskyi, O. V. Leshko, M. A. Slusarenko, Micro Nanostructures **181**, 207615 (2023); https://doi.org/10.1016/j.micrna.2023.207615.

[15] G. Zaiats et al., Z. Phys. Chem. **229**, 3 (2015); https://doi.org/10.1515/zpch-2014-0625.

[16] R. Ya. Leshko, O. V. Leshko, I. V. Bilynskyi, V. B. Holskyi, Opt. Commun. **566**, 130722 (2024); https://doi.org/10.1016/j.optcom.2024.130722.

[17] D. J. BenDaniel, C. B. Duke, Phys. Rev. **152**, 683 (1966); https://doi.org/10.1103/PhysRev.152.683.

[18] O. von Roos, Phys. Rev. B **27**, 7547 (1983); https://doi.org/10.1103/PhysRevB.27.7547.

[19] C. Quesne, V. M. Tkachuk, J. Phys. A **37**, 4267 (2004); https://doi.org/10.1088/0305-4470/37/14/006.

[20] V. M. Tkachuk, O. Voznyak, Eur. Phys. J. Plus. **130**, 161 (2015); https://doi.org/10.1140/epjp/i2015-15161-x.

[21] Shu-Shen Li, Jian-Bai Xia, Chin. Phys. Lett. **23**, 1896 (2006); https://doi.org/10.1088/0256-307X/23/7/066.

[22] Shu-Shen Li, Jian-Bai Xia, J. Appl. Phys. **101**, 093716 (2007); https://doi.org/10.1063/1.2734097.

R. Ya. LESHKO, O. V. LESHKO, I. V. BILYNSKYI, R. I. PAZYUK

ЕЛЕКТРОН-ДІРКОВА ОБМІННА ВЗАЄМОДІЯ В НЕКОНЦЕНТРИЧНИХ СФЕРИЧНИХ КВАНТОВИХ ТОЧКАХ ТИПУ ЯДРО-ОБОЛОНКА

Р. Я. Лешко[1], О. В. Лешко[1], І. В. Білинський[1,2], Р. І. Пазюк[1]

[1] *Кафедра фізики та інформаційних систем, Дрогобицький державний педагогічний університет імені Івана Франка, вул. Стрийська, 3, Дрогобич, 82100, Україна,*

[2] *Кафедра фізики, Криворізький державний педагогічний університет, просп. Університетський, 54, Кривий Ріг, 50086, Україна*

У роботі теоретично досліджено вплив параметра нецентричності на величину розщеплення темного та світлого станів екситонів у сферичних квантових точках CdSe/CdS типу ядро-оболонка зі зміщеним ядром від спільного центра. Розглянуто квантові точки з різною товщиною оболонок: як тонкими, так і широкими. Особливу увагу приділено впливу неконцентричності, тобто зміщенню ядра від спільного центра квантової точки, на енергію електрон-діркової обмінної взаємодії, тобто на розщеплення темного та світлого екситонних станів. Для опису системи використано метод ефективної маси, що враховує відмінності в масах електронів і дірок у матеріалах ядра та оболонки, а також модель прямокутних потенціальних ям і бар'єрів. Ця модель є однією з найпростіших, але водночас ефективною для опису поведінки носіїв заряду в наноструктурах типу ядро-оболонка. Відповідні рівняння Шредінґера для електрона й дірки в межах цієї моделі розв'язано за допомогою методу розкладу за плоскими хвилями. Це дає змогу точно врахувати вплив різних геометричних параметрів квантової точки на енергетичний спектр і на просторовий розподіл хвильових функцій носіїв заряду. У підсумку розрахунків показано, що зі збільшенням радіуса оболонки енергія електрон-діркової обмінної взаємодії зменшується, що зменшує розщеплення темного і світлого станів екситонів. Це можна пояснити збільшенням відстані між хвильовими функціями електрона й дірки у великих оболонках, що знижує їхнє перекриття і, відповідно, енергію обмінної взаємодії. Окрім того, за фіксованих розмірів ядра та оболонки виявлено, що зміщення ядра від спільного центра квантової точки має різний вплив залежно від радіуса оболонки. Для малих радіусів оболонки спостерігаємо монотонне збільшення енергії обмінної взаємодії зі збільшенням нецентричності, тоді як для більших радіусів ця залежність стає немонотонною. Це пояснюємо складнішим перекриттям хвильових функцій у системах з великими оболонками, де хвильові функції електрона й дірки можуть мати складний розподіл у просторі. Отримані результати добре узгоджуються з експериментальними даними.

Ключові слова: спектри сонячних спалахів, обробка астрономічних зображень, обчислення на графічних процесорах, аналіз астрономічних даних, спектроскопіяквантова точка типу ядро-оболонка, параметр неценттричності, розщеплення темних та світлих станів екситона.